The Astronomical Journal, 124:706–721, 2002 August

COMPLEX FORMATION HISTORY OF THE LENTICULAR GALAXIES WITH STELLAR COUNTERROTATION: NGC 4138 AND NGC 4550[1]

V. L. Afanasiev
Special Astrophysical Observatory, Nizhnij Arkhyz, 369167 Russia; vafan@sao.ru

and

O. K. Sil'chenko[2]
Sternberg Astronomical Institute, Moscow, 119992 Russia; and Isaac Newton Institute of Chile, Moscow Branch; olga@sai.msu.su

Received 2001 June 14; accepted 2002 March 24

ABSTRACT

Two lenticular galaxies with counterrotating stellar components in their disks have been studied with the Multi-Pupil Fiber Spectrograph of the 6 m telescope (at the Special Astrophysical Observatory). In NGC 4138 the nucleus is certainly chemically distinct, with the central concentration of magnesium enhancement marginally exceeding that of iron. The ionized gas within $R = 4''$ of the nucleus rotates circularly in an inclined ring, perhaps a kind of a circumnuclear polar ring surrounding a compact stellar minibar. NGC 4550 exhibits complex extended structures in its center that can be identified by enhanced levels of magnesium and iron indices; the stellar population of the unresolved nucleus is younger than that of the circumnuclear region. We conclude that although NGC 4550 does not possess a chemically distinct nucleus in the ordinary sense of the term, there are nevertheless clear signatures of a secondary star formation burst confined perhaps to the counterrotating stellar gaseous disk. We argue that the inclination of the counterrotating disk differs from that of the main stellar disk, implying that the two disks are not coplanar. Both galaxies seem to have possessed bars, either actually present or already dissolved.

Key words: galaxies: evolution — galaxies: individual (NGC 4550, NGC 4138) — galaxies: nuclei — galaxies: structure

1. INTRODUCTION

It was back in 1992 that we first reported the existence of chemically distinct (metal enriched) stellar nuclei in early-type disk galaxies (Sil'chenko, Afanasiev, & Vlasyuk 1992). A preliminary statistical analysis implied that as much as half of all Sa or Sb galaxies and at least a quarter of all SOs may possess such nuclei (Sil'chenko 1994). We now know about two dozen well-studied cases. Recently a new French-Dutch-British project of the two-dimensional spectrograph SAURON has started at the 4.2 m William Herschel Telescope (WHT), and one of the first attempts to map absorption-line indices in the centers of nearby early-type galaxies has led to a discovery of a chemically distinct nucleus in NGC 3384 (de Zeeuw et al. 2002). What may be an origin of the chemically distinct nuclei? We noted that the phenomenon of chemically distinct nuclei is often accompanied by that of multiple kinematical subsystems. For example, we found chemically distinct nuclei in NGC 7331 (Sil'chenko 1999b) and NGC 7217 (Sil'chenko & Afanasiev 2000) where counterrotating stellar subsystems had been reported earlier by Prada et al. (1996) and Merrifield & Kuijken (1994), respectively, as well as in NGC 4826 (Sil'chenko 1996) and NGC 7332 (Sil'chenko 1999a), which contain counterrotating gas (Rubin 1994; Rix et al. 1995; Fisher, Illingworth, & Franx 1994; Plana & Boulesteix 1996). As for a very regular Sb galaxy NGC 2841, we began by finding there a chemically distinct nucleus and a circumnuclear polar gaseous disk (Sil'chenko, Vlasyuk, & Burenkov 1997b), followed by a counterrotating stellar component, which we later discovered in its bulge (Afanasiev & Sil'chenko 1999). Circumnuclear polar gaseous disks in noninteracting spiral galaxies are quite a new phenomenon, which might also be related to chemically distinct nuclei; besides NGC 2841, we found them in NGC 6340 (Sil'chenko 2000) and NGC 7217 (Zasov & Sil'chenko 1997; Sil'chenko & Afanasiev 2000). Chemically distinct nuclei might be in some way genetically related to multiple kinematical subsystems. To further explore this idea, we undertook a special study of stellar population properties in the centers of two early-type disk galaxies with counterrotating global stellar disks: NGC 4138 and NGC 4550. Table 1 summarizes the global parameters of these galaxies.

The most comprehensive analysis of the regular S0/a galaxy NGC 4138 has been performed by Jore, Broeils, & Haynes (1996), who investigated the H I distribution and kinematics, broadband (*I* filter) morphology, and differential photometry, and made long-slit kinematic observations of stars and ionized gas, which make up the most impressive part of their work. The above authors found that gas—both neutral and ionized—counterrotates with respect to the major stellar component; however, there is also a counterrotating stellar component, which exhibits disklike velocity dispersion and is concentrated toward the gaseous ring of radius $22''$ (1.7 kpc). Also noteworthy are line-of-sight velocity variations along the minor axis shown by the ionized gas within $\pm 5''$ of the center: even though the whole counterrotating matter is confined to the global galactic disk as Jore et al. (1996) argue, there is a violation of circular

[1] Partly based on observations collected with the 6 m telescope (BTA) at the Special Astrophysical Observatory of the Russian Academy of Sciences.

[2] Guest investigator of the UK Astronomy Data Centre.

TABLE 1
GLOBAL PARAMETERS OF THE GALAXIES

Parameter	NGC 4138	NCG 4550
Type (NED)	SA(r)0$^+$	SB0
R_{25} (kpc) (LEDA)	6.4	8.1
B_T^0 (RC3)	12.08	12.36
M_B	−18.94	−18.7
$(B-V)_T^0$ (RC3)	0.83	0.84
$(U-B)_T^0$ (RC3)	0.31	0.38
V_r(radio) (LEDA) (km s^{-1})	907	381
Distance, Mpc (LEDA, $H_0 = 75$ km s^{-1} Mpc^{-1})	14.6	17 (Virgo)
Inclination (LEDA) (deg)	61	90
P.A.$_{\rm phot}$ (LEDA) (deg)	150	178

character of rotation or of a well-settled planar distribution in the very center. It also remains to carefully verify the results of the photometric analysis by Jore et al. (1996), who claim NGC 4138 ($B/D = 0.13$) to be a globally disk-dominated galaxy despite its very early morphological type. The *I*-band brightness profile of NGC 4138 reported by Jore et al. (1996) fits well a single exponential law at $R > 10''$, and the bulge of the galaxy is very compact and also exponential. At the same time Baggett, Baggett, & Anderson (1998) analyzed the *V*-band brightness profile of NGC 4138 and found a much more prominent de Vaucouleurs bulge with $r_e = 22''$ and an inner cutoff of the exponential disk at $R = 19''$. The morphology of the galaxy remains quite unclear. We must add only that the galaxy possesses a ring of H II regions at $R \approx 22''$ (Pogge & Eskridge 1987) while being morphologically unbarred.

NGC 4550 is an S0 galaxy seen almost edge-on. Rubin, Graham, & Kenney (1992) have noted in it two counter-rotating stellar disks of comparable strength. Rix et al. (1992) carefully analyzed a long-slit major-axis spectrum of this galaxy and showed its counterrotating stellar components to have identical exponential radial brightness distributions at $R > 6''$ and uniformly low stellar velocity dispersion of less than 60 km s^{-1}. Though the disky nature of both counterrotating stellar components is beyond doubt, the morphology of this galaxy remains ambiguous, as is that of NGC 4138. Rix et al. (1992) and Fisher, Franx, & Illingworth (1996) noted a small de Vaucouleurs bulge seen only inside $R \approx 5''$, with B/T estimates ranging from 0.16 to 0.3; Gavazzi et al. (2000) confirmed the predominance of the global disk component ($B/T = 0.21$) but reported an exponential radial brightness distribution in the bulge in the *H* filter. However, the sophisticated two-dimensional decomposition of the *V*-image of NGC 4550 by Scorza et al. (1998) yielded an exponential disk fully embedded into a de Vaucouleurs bulge and everywhere fainter than the latter (the total $B/D \approx 5$); similar results were obtained by Baggett et al. (1998), who analyzed a one-dimensional *V*-band brightness profile in terms of exponential and de Vaucouleurs law for the disk and bulge, respectively: the disk was found to be everywhere fainter than the bulge. Finally Simien & Michard (1990) and Caon, Capaccioli, & D'Onofrio (1993) concluded that the brightness profile of the dominant component in NGC 4550, be it bulge or disk, is neither exponential nor de Vaucouleurs; it can be best fitted by the Sersic law with $n = 1.7$. After all, we do not yet know whether this galaxy is disk- or bulge-dominated; if the latter is true, the question arises immediately: Why do Rix et al. (1992) see no kinematical signatures of the bulge along the major axis? The very center of the galaxy within $R = 3''$ (Rix et al. 1992) also exhibits a rather unusual kinematical behavior: the stellar component with a zero rotation velocity and a velocity dispersion of only 80 km s^{-1} combined with rather rapidly rotating ionized gas. Where is the kinetic energy of stars? Is the system not virialized?

2. OBSERVATIONS AND DATA REDUCTION

The spectral data that we analyze in this work were obtained with three different integral field spectrographs. Integral field spectroscopy is a rather new approach, which was first suggested by G. Courtes some 15 years ago (see Bacon et al. 1995 for a description of the underlying idea of the instrument). This technique allows one to obtain simultaneously a set of spectra covering a wide spectral interval from an extended sky area, for example, from a central part of a galaxy. A two-dimensional array of microlenses provides a set of micropupils, which are put onto to the entry of a spectrograph. A reduction of a full set of spectra corresponding to individual spatial elements yields a list of continuum and emission-line fluxes, line-of-sight velocities for stars and ionized gas, and equivalent widths of absorption lines, which are usually expressed as indices in the well-defined Lick system (Worthey et al. 1994). The resulting list can be transformed into two-dimensional maps of the parameters mentioned above for the central part of the galaxy under study. This approach offers, besides the well-known benefits of field observations, a unique opportunity to superpose various two-dimensional distributions without bothering about positioning problems. Two spectral ranges are usually exposed, green (4800–5600 Å) and red (6200–6900 Å). The green spectra are used to calculate the Lick indices Hβ, Mg *b*, Fe 5270, and Fe 5335, which are suitable for determining metallicity, age, and the Mg/Fe ratio of old stellar populations (Worthey 1994), and to cross-correlate the galaxy spectra with the spectrum of a template star, usually of a K0 III–K3 III spectral type, to derive the line-of-sight velocity field for the stellar component and in some cases the map of stellar velocity dispersion. The red spectral range contains the strongest optical emission lines Hα and [N II] λ6583, which are used to derive the line-of-sight velocity field of ionized gas. The detailed log observations of NGC 4138 and NGC 4550 galaxies made with three different two-dimensional spectrographs is given in Table 2.

The observations in 1998 January were made with the old variant of the Multi-Pupil Field Spectrograph (MPFS) of the 6 m telescope (Afanasiev et al. 1996). The instrument operated in two modes with 8×12 or 8×16 micropupil arrays, supported by 520×580 and 1040×1160 CCD detectors, respectively, with a spatial scale of $1''.3$ per microlens and a reciprocal dispersion of 1.6 Å per pixel (the spectral resolution was 4–6 Å and varied slightly over the frame). We performed wavelength calibration by using separate exposures for the spectrum of the hollow-cathode lamp filled with helium, neon, and argon; the internal accuracy of linearization was typically 0.25 and 0.1 Å in the green and red ranges, respectively. However, we checked the accuracy and absence of systematic shifts in the velocity scale by measuring strong night-sky emission lines [O I] λ5577 and [O I] λ6300. In this variant of two-dimensional

TABLE 2
TWO-DIMENSIONAL SPECTROSCOPY OF NGC 4138 AND NGC 4550

Date	Galaxy	Exposure (min)	Configuration	Field	Spectral Range (Å)	Seeing
1998 Jan 21	NGC 4138	60	BTA/MPFS+CCD 520 × 580	10″ × 16″	4700–5400	2.″4
1998 Jan 23	NGC 4550	40	BTA/MPFS+CCD 1040 × 1160	11″ × 21″	4200–5600	2.″2
1999 Jun 6	NGC 4550	60	BTA/MPFS+CCD 1024 × 1024	16″ × 15″	4200–5600	1.″7
1999 Jun 9	NGC 4550	30	BTA/MPFS+CCD 1024 × 1024	16″ × 15″	5800–7200	2.″5
1999 Dec 12.....	NGC 4138	45	BTA/MPFS+CCD 1024 × 1024	16″ × 15″	4200–5600	3.″0
1999 Dec 15.....	NGC 4138	45	BTA/MPFS+CCD 1024 × 1024	16″ × 15″	5800–7200	2.″1
1999 Feb 21	NGC 4550	120	WHT/SAURON+CCD 2000 × 4000	33″ × 41″	4800–5400	3.″0

spectroscopy, we also made a separate exposure of a blank sky area several arcminutes from the galaxy, because we needed sky subtraction to calculate properly the equivalent widths of the absorption lines. We checked the consistency of our index system with the Lick system by observing nine standard stars from the list of Worthey et al. (1994) and found our indices to be in excellent agreement with those tabulated by the above authors, with the mean deviations being less than 0.05 Å.

Later in 1998, a new variant of the MPFS became operational in the prime focus of the 6 m telescope.[3] Compared with the old variant, the new MPFS has a larger field of view and wider total spectral range. This became possible because of the use of optical fibers transmitting to the spectrograph slit the light from 16 × 15 square elements of the galaxy image and another 16 fibers transmitting sky background light taken outside the galaxy, thus eliminating the need for separate sky exposures. The size of one spatial element was approximately 1″ × 1″. The detector used was 1024 × 1024 TK CCD with a reciprocal dispersion of 1.35 Å per pixel and a rather stable spectral resolution of 5 Å. The wavelength calibration was performed in the same way as in the previous variants of the MPFS observations. To calibrate the new MPFS index system onto the standard Lick one, we observed 15 stars from the list of Worthey et al. (1994) during four observational runs. Figure 1*a* compares the indices calculated directly from the new MPFS spectra with those tabulated in Worthey et al. (1994). The data points can be seen to form tight linear relations, which, however, deviate slightly from bisectors. We have calculated the linear regression formulae to transform our index measurements into the Lick system; the rms scatter of data points in Figure 1*a* about these linear relations is ~0.2 Å for all four indices considered and is therefore within the observational errors quoted by Worthey et al. (1994). We corrected our index measurements for the broadening due to stellar velocity dispersion, which usually differs substantially from zero in the centers of early-type galaxies. We determined the correction values by artificial Gaussian broadening of the spectrum of the standard star HD 97907 by using various σ values. We then fitted fourth-order polynomials to the derived dependencies of index corrections on σ and applied the resulting corrections to the measured index values prior to reducing them into the Lick system. A typical correction for stellar velocity dispersion is about 0.4 Å in the spectral index at $\sigma = 200$ km s^{-1}.

The third two-dimensional spectrograph whose data we use in this work is the new SAURON instrument operated at the 4.2 m William Herschel Telescope of La Palma Observatory (see Bacon et al. 2001 for a detailed description). We retrieved the data for NGC 4550 obtained with this instrument in 1999 February from the open Isaac Newton Group (ING) Archive of the UK Astronomy Data Centre. This instrument has a field of view of 41″ × 33″ and each spatial element has size 0.″94 × 0.″94. Sky background is exposed simultaneously with the target object 2′ from the center of the galaxy. The data cover the spectral range 4800–5400 Å with a reciprocal dispersion of 1.11–1.21 Å, which varies from the left to the right edge of the frame. Neon spectrum is used for comparison and linearization is performed to an accuracy of 0.1 Å by using a second-order polynomial. The consistency of the resulting index system with the Lick system is checked using seven stars from the list of Worthey et al. (1994). Figure 1*b* compares the indices measured directly from the SAURON spectra with the values tabulated by Worthey et al. (1994). The two index systems agree to within an rms scatter of 0.3 Å, and therefore we apply no correction to the index system, based on the SAURON data. This example demonstrates that index systems usually depend on the shape of the continuum rather than on spectral resolution: the spectral resolution of SAURON, which is equal to 3.5 Å, differs more from the standard Lick resolution of 8 Å than does that of the new MPFS of 5 Å, whereas the SAURON index system is closer to the standard one, perhaps because of the flat spectral response of the instrument.

The exposure times for the galaxies observed with both variants of the MPFS were chosen to be long enough to achieve signal-to-noise ratios of no less than 60 (per angstrom unit) in the nuclei and ≤20 near the frame edges; according to Cardiel et al. (1998), this level of signal-to-noise ratio provides an accuracy of line indices ranging from 0.15 Å in the center to 0.6 Å for the individual spatial elements in the outer part of the galaxy. To keep the accuracy constant along the radius, we also co-added the element spectra obtained with every two-dimensional spectrograph within concentric circular rings centered on the nuclei and then studied the radial dependencies of the stellar population properties by comparing our azimuthally averaged absorption-line indices to evolutionary synthesis models of old stellar populations by Worthey (1994). We estimate the typical accuracy of our azimuthally averaged indices to be better than 0.1 Å.

For NGC 4138 we used in addition to the two-dimensional spectral data some photometric data, namely, the 200 + 160 s exposures made with the *Hubble Space Telescope* Wide Field Planetary Camera 2 (*HST* WFPC2) on 1997 July 7, using the F547M, which we retrieved from

[3] See http://www.sao.ru/~gafan/devices/mpfs/.

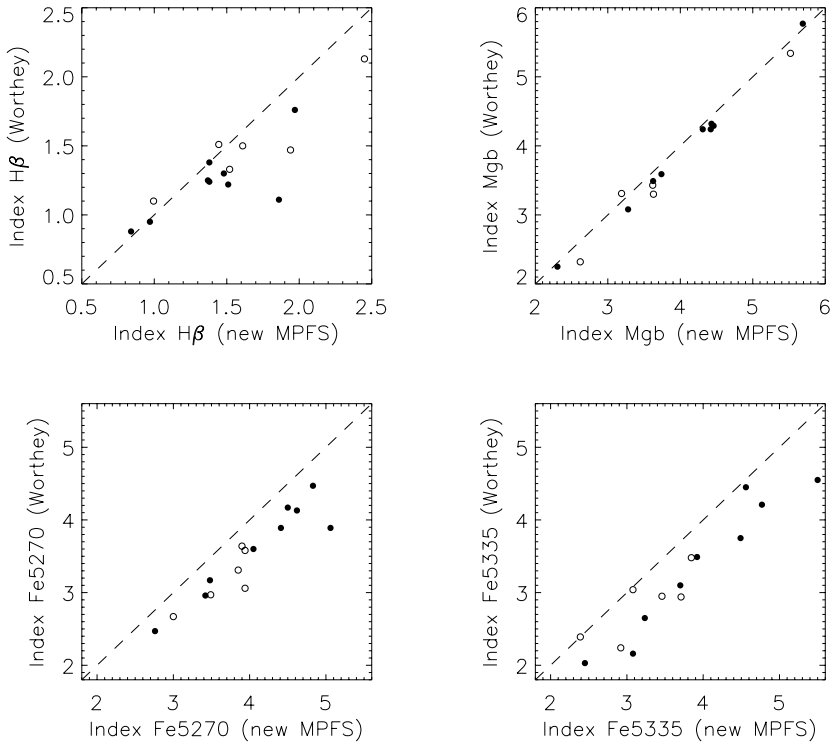

FIG. 1*a*

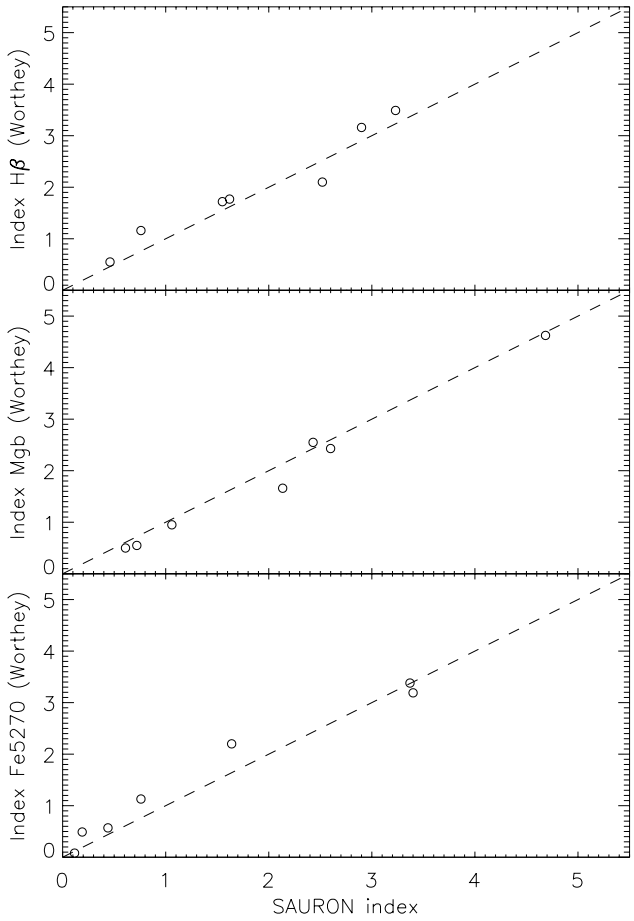

FIG. 1*b*

FIG. 1.—Calibration of our measured indices into the Lick system by using observations of standard stars: (*a*) new MPFS (starting from 1999). Different symbols correspond to different observing seasons. (*b*) 1999 February SAURON data. Dashed lines show quadrant bisectors.

the *HST* Archive, and broadband *BRIK* images of the galaxy obtained within the framework of the Ursa Major Cluster Survey of Tully, which we adopted from the CD-ROM collection of the Canadian Astronomy Data Center.

All the data, spectroscopic and photometric, except those obtained with the new MPFS, were reduced with the software developed by V. V. Vlasyuk in the Special Astrophysical Observatory (Vlasyuk 1993). Primary reduction of the data obtained with the new MPFS was performed using IDL-based software developed by one of us (V. L. A.). The Lick indices were calculated with our own FORTRAN program and a FORTRAN program of A. Vazdekis.

3. NGC 4138

3.1. *Nuclear and Circumnuclear Stellar Populations*

We measured radial variations of the Lick indices Hβ, Mg *b*, Fe 5270, and Fe 5335 in the central part of NGC 4138 twice, in 1998 January with the old MPFS operating with a 8×12 microlens array and in 1999 December with the new MPFS and a 16×15 microlens array. Figure 2 compares two sets of azimuthally averaged measurements within $R = 9''$. No significant systematic discrepancies between index measurements are in evidence here despite quite different spectrographs and slightly different spectral resolutions. Both sets of measurements yield rather accurate indices, and one can even note the poorer spatial resolution in 1999 December to show up in the Mg *b* profile.

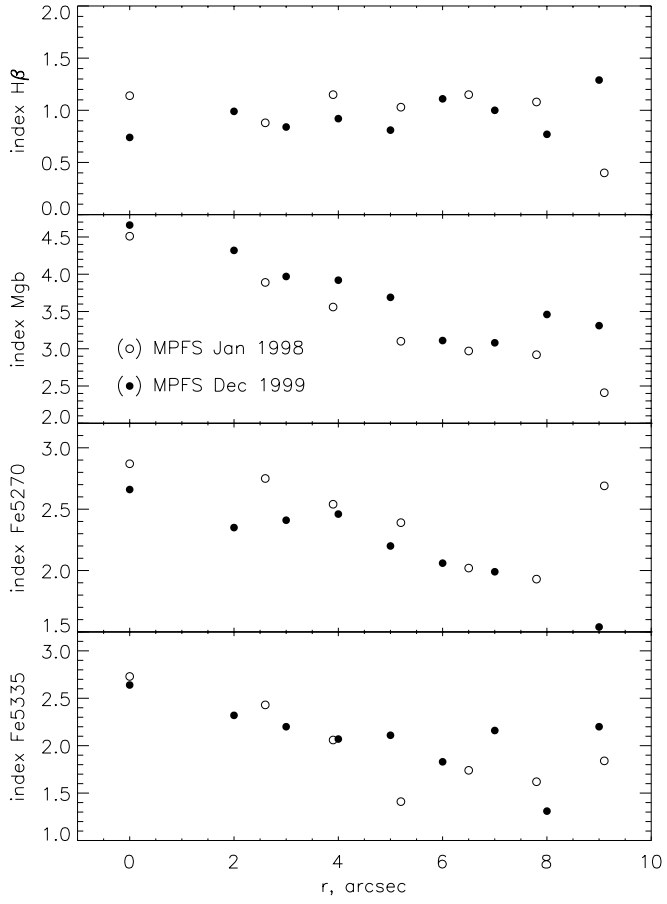

FIG. 2.—Comparison of two MPFS sets of index measurements for NGC 4138. Two-dimensional measurements are azimuthally averaged over concentric rings centered onto the nucleus.

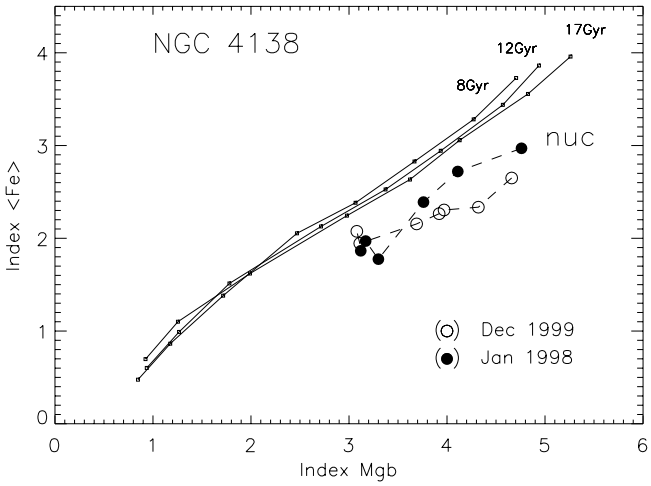

FIG. 3.—Iron vs. magnesium diagram for azimuthally averaged index measurements in NGC 4138. The data points are taken in galactocentric radial steps of 1.″3 and 1″ for the 1998 January and 1999 December sets, respectively. The models of Worthey (1994) for old stellar populations with [Mg/Fe] = 0 are plotted as a reference; the metallicities of Worthey's models are (*top to bottom*) +0.50, +0.25, 0.00, −0.22, −0.50, −1.00, −1.50, and −2.00.

Figure 3 shows a diagram of $\langle$Fe$\rangle$ versus Mg *b* [$\langle$Fe$\rangle \equiv$ (Fe 5270 + Fe 5335)/2], where we compare our measurements to simple models of old stellar populations by Worthey (1994). The indices are already corrected for the broadening due to stellar velocity dispersion as measured by Jore et al. (1996). One can see that the radial variations of metal indices in NGC 4138 are roughly parallel to model sequences, implying that the stellar populations in the center of NGC 4138 are mildly magnesium-overabundant ([Mg/Fe] $\approx +0.2$), and this magnesium-to-iron ratio remains almost constant along the radius. The behavior is similar to that of giant elliptical galaxies (Worthey, Faber, & Gonzalez 1992), although NGC 4138 is more often classified as an S0–Sa galaxy and its bulge is of a very moderate luminosity. Unfortunately, the strong contamination by emission prevents the use of the Hβ index for determining the mean age of stellar population and disentangling age and metallicity effects in this particular case. Nonetheless, strong nucleus-to-bulge variations of mean metallicity show up in the $\langle$Fe$\rangle$ versus Mg *b* diagram: the nucleus and the bulge are closer to the models with above-solar and subsolar metallicities, respectively. If we assume that the ring at $R = 5''$–$7''$, taken as a representative bulge area, lies beyond the region affected by the nucleus under our moderate seeing quality, the nucleus-to-bulge metal index differences are ΔMg $b = 1.44 \pm 0.20$ and $\Delta\langle$Fe$\rangle = 0.92 \pm 0.13$, corresponding to a total metallicity difference of 0.6 dex, or a factor of 4, if equal mean ages are assumed for both stellar populations. A relatively younger nucleus compared with the bulge, which is typical for chemically distinct nuclei (Sil'chenko 1999a, 1999b; Sil'chenko & Afanasiev 2000), should imply an even greater metallicity difference.

Figure 4 demonstrates two-dimensional maps of the Lick indices Hβ, Mg *b*, and $\langle$Fe$\rangle$ for the small central region of NGC 4138 according to our MPFS measurements of 1999 December smoothed by a Gaussian with FWHM = 2.″3.

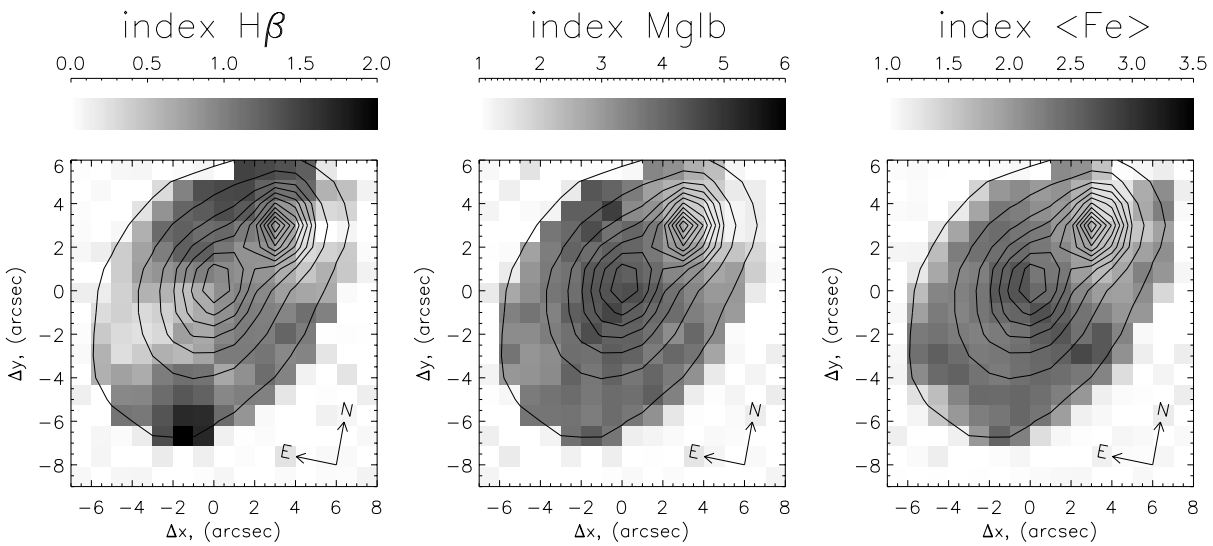

FIG. 4.—MPFS index maps for NGC 4138. Green (λ5000 Å) continuum is superposed by isophotes; the second brightness peak northwest of the nucleus is due to a foreground star.

The map of Hβ absorption-line index tells us little about the properties of stellar populations: throughout the entire central region of NGC 4138 it is contaminated by Balmer emission, and the strongest contamination is observed near the major axis of the continuum isophotes. But as far as metal line indices are concerned, both Mg *b* and ⟨Fe⟩ maps reveal the chemically distinct nature of the nucleus (the second continuum brightness peak on the major axis northwest of the nucleus and the corresponding minima in all indices are due to a bright blue foreground star). However, the Mg *b* and ⟨Fe⟩ indices can be seen to exhibit different behaviors: magnesium is centrally peaked, whereas the maximum of the iron index shows up as a resolved elongated feature. We have already seen similar "iron-rich circumnuclear disks" in galaxies with chemically distinct nuclei, e.g., in the S0 galaxy NGC 1023 (Sil'chenko 1999a) or in the Sb galaxy NGC 7331 (Sil'chenko 1999b), but it is for the first time that this structure is elongated in a direction close to the minor axis of the continuum isophotes.

3.2. *Central Kinematics of Stars and Ionized Gas*

Jore et al. (1996) performed a detailed analysis of the kinematics of stars and ionized (as well as neutral) gas in this galaxy, but this work is based only on observations made with a long slit oriented along the major and minor axes. We used a two-dimensional field spectrograph, and therefore our results shed additional light onto the peculiar kinematics of NGC 4138.

Figure 5 shows two-dimensional velocity fields for stars and ionized gas (the latter is based on [N II] λ6583 emission-line measurements). Both velocity fields look quite regular: stars demonstrate a rigid rotation pattern, and the rotation of ionized gas shows marginal local maxima of relative

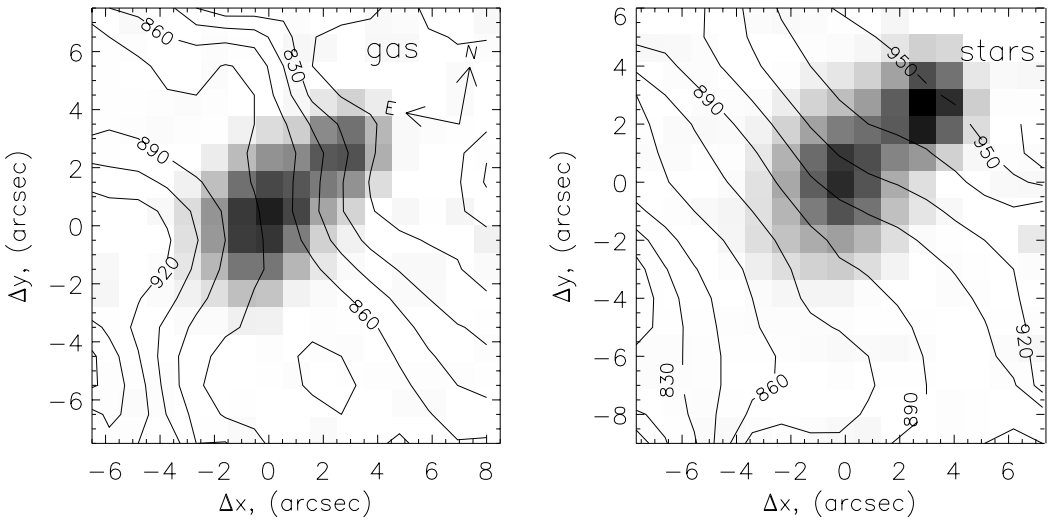

FIG. 5.—Line-of-sight velocities of the stellar and gaseous components in the center of NGC 4138 (*isolines*), superposed on the green and red continuum images.

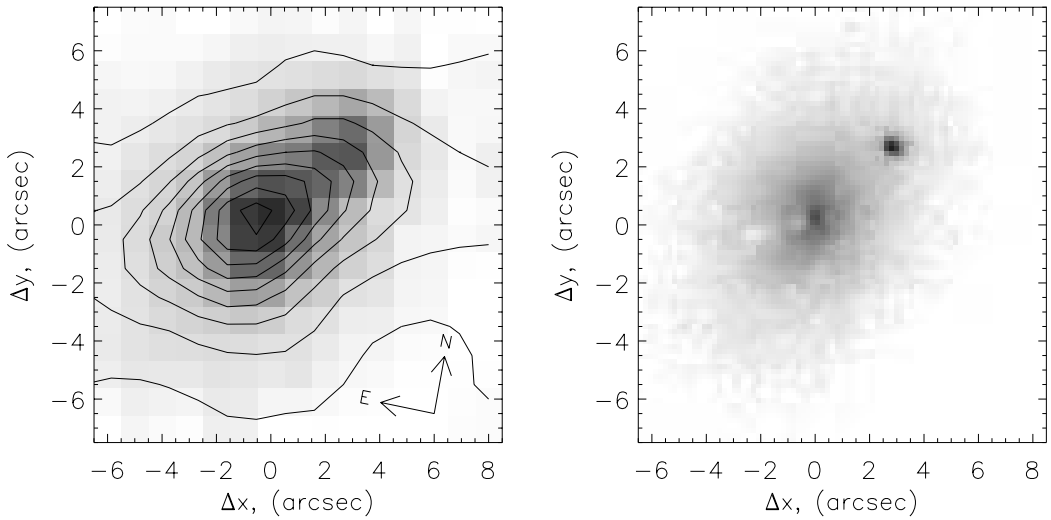

FIG. 6.—[N II] λ6583 emission-line surface brightness distribution (*isolines*) superposed on the red (λ6500) continuum image in the center of NGC 4138 (*left*) and for comparison an *HST* WFPC2 image at the same scale and with the same orientation (*right*).

velocity 5″–6″ from the center. In a rough sense, stars and ionized gas counterrotate, as reported by Jore et al. (1996): the receding side of the stellar rotation curve is the one northwest of the center, and that of the gas rotation curve, southeast of the center. But we now report a feature that is of greatest, we would even say crucial, importance: the kinematical major axis (the direction of maximum line-of-sight velocity gradient) of the stellar subsystem does not coincide with this of the ionized gas subsystem, implying that the two systems may rotate in different planes. Averaging over two measurement sets and three radial bins yields for stars a kinematical major-axis orientation of $\mathrm{P.A.}_{0,*} = 327^\circ \pm 3^\circ$ in the 2.″5–5″ radial interval. The fact that the line of nodes of the galactic global disk inferred from the orientation of the outermost isophotes does not deviate strongly from this direction (330° and 332° according to the Lyon-Meudon Extragalactic Database [LEDA] and to our own photometric measurements reported in § 3.3., respectively) leads us to conclude that stars within $R = 3''$–$5''$ rotate axisymmetrically in the global symmetry plane of NGC 4138. As for ionized gas, its kinematical major axis in the same radius range has a position angle of $\mathrm{P.A.}_{0,g} = 116^\circ \pm 4^\circ$ (according to the line-of-sight velocity fields based on [N II] λ6583 and [O III] λ5007 emission-line measurements) and thus deviates by 35° from the line of nodes.

To what plane can we attribute this circumnuclear ionized gas? Or does it experience strong noncircular motions? Figure 6 (*left*) shows the surface brightness distribution in the [N II] λ6583 emission line. The major axis of the innermost emission-line isophotes has a position angle of P.A. ≈ 113°, which is very close to that of the kinematical major axis [the emission isophote deviation from the line of nodes is even more pronounced in the more outer part at $R > 7''$, where P.A.(major axis) ≈ 100°]. The coincidence of the kinematical and photometric major axes is indicative of planar axisymmetric rotation. The central angular rotation velocity of stars, as estimated from the velocity field shown in Figure 5, is $\omega \sin i = 11.3 \pm 0.7$ km s^{-1} arcsec^{-1}; the maximum central line-of-sight velocity gradient for ionized gas is 12.3 ± 1.6 km s^{-1} arcsec^{-1}. The comparable velocity dispersions of stars and ionized gas (∼150 and ∼120 km s^{-1}, respectively; Jore et al. 1996) in the center of NGC 4138 and the fact that the inclination of the gaseous disk implied by the ellipticity of the emission-line isophotes shown in Figure 6 (*left*) does not differ strongly from that of the global stellar rotation plane lead us to interpret the coincidence of the maximum central line-of-sight velocity gradients for stellar and ionized gas subsystems as conclusive evidence of circumnuclear ionized gas being confined to and rotating circularly in a plane inclined with respect to the global symmetry plane of the galaxy. This point can be illustrated by an F547W-band image of the central part of NGC 4138 obtained with the *HST* WFPC2 (Fig. 6, *right*). One can see a straight dust lane crossing the center of the galaxy and extending to a radius of at least 3″; the orientation of this dust lane is P.A. = 115°—the same as that of the kinematical and photometric major axes of the gaseous emission. The circumnuclear gaseous disk appears to contain a significant amount of dust. The overall appearance of Figure 6 (*right*) gives the impression that the dust lane crosses the central elongated structure at a right angle. If so, continuum isophotes should be strongly twisted in the center. Or perhaps this might be a false impression caused by the complex distribution of dust? To answer this question, in the next subsection we analyze the photometric structure of NGC 4138

3.3. *Photometric Structure*

To investigate the photometric structure of NGC 4138, we used *BRIK* images of the galaxy taken from the survey of the Ursa Major Cluster of galaxies by Tully (CD-ROM collection at Harvard). The images were taken under good seeing conditions, $\mathrm{FWHM}_* = 0.''8/0.''9$, and their analysis can reveal a number of interesting details. Figure 7 shows the variations of isophotal characteristics along the radius. One can see that both the position angle of the major axis and the ellipticity remain more or less constant at $R > 25''$, and we therefore may adopt these asymptotic values (the position angle of the line of nodes of $\mathrm{P.A.}_0 \approx 150^\circ$ and the inclination of about 50°, which corresponds to an ellipticity of 0.36) for the entire global stellar disk. Inside $R = 25''$ meas-

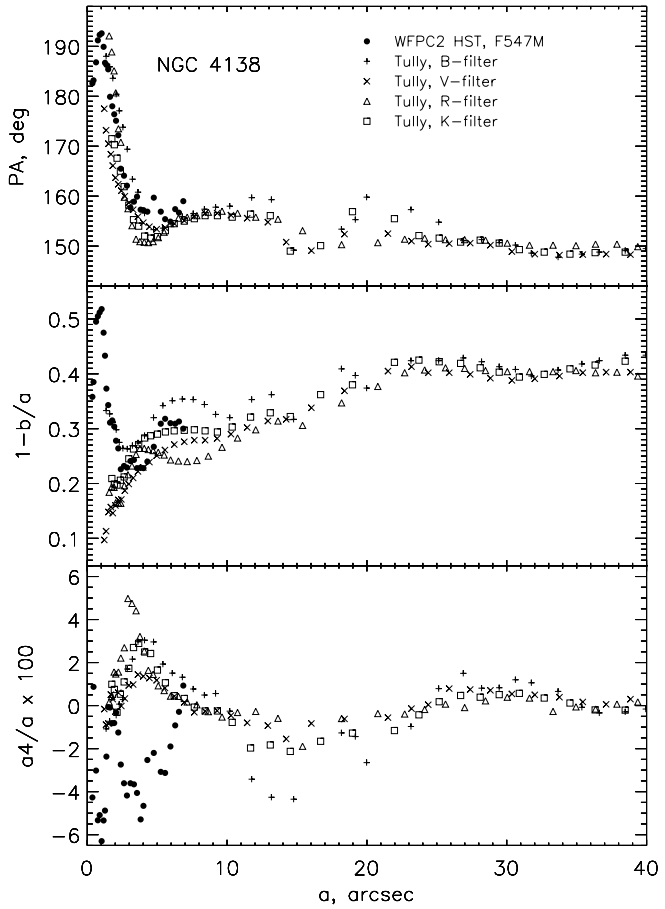

FIG. 7.—Radial variations of isophote parameters in NGC 4138

urements made in different passbands are somewhat discrepant in the systematic sense; these data must be obviously affected by the large amount of dust, with the *K*-band measurements being the least sensitive. Strong variations of the isophote parameters are observed inside $R = 3''$. The blue-band isophote ellipticity increases toward the nucleus and we may interpret this rise as a dust effect. However, the major axis verges to the north-south direction consistently in all filters, implying that this turn cannot be interpreted in terms of clumpy absorption. The position angle of the circumnuclear continuum isophotes is close to P.A. $\approx 13^\circ$, leading us to conclude that the galaxy should have a compact circumnuclear minibar or a minidisk around which a quasi-polar gaseous ring rotates (because $\mathrm{P.A.}_{0,g} \approx 115^\circ$; see § 3.2).

We averaged surface brightness over elliptical rings with P.A. $= 152^\circ$ and $1 - b/a = 0.36$ and fitted the outer part of the profile within galactocentric distances of $R = 25''$–$67''$ by an exponential law. We found that at $R > 8''$ the galaxy is dominated by a global exponential disk; the exponential scale length of this disk varies from $16''.3$ in *B* to $13''.8$ in *K*, which is consistent with the *I*-band scale length of $15''.8 \pm 0''.1$ (Jore et al. 1996). The central surface brightness, $B_0 = 19.9$, is very high compared with the canonical value of 21.7 for most of the disk galaxies (Freeman 1970). Figure 8 shows the residual *K*-band image after subtracting the global exponential disk; the residual map is deprojected onto the galactic plane with the line of nodes lying horizontally. A prominent stellar ring is immediately apparent at

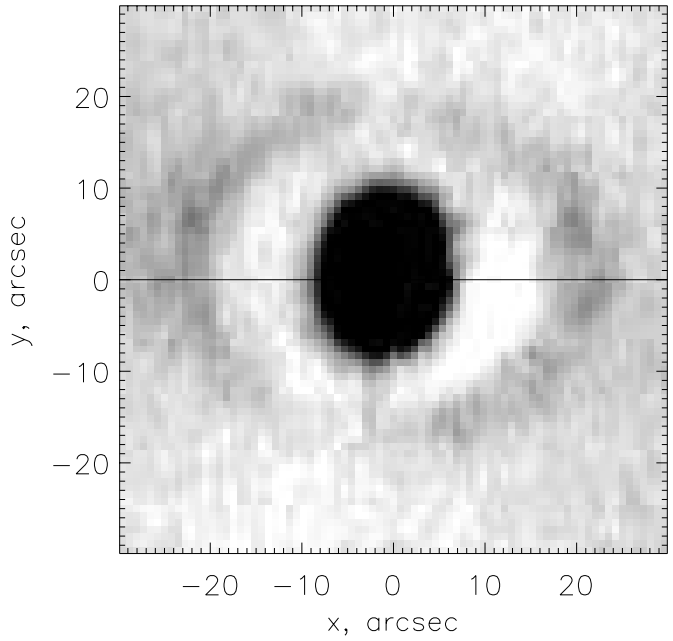

FIG. 8.—Residual *K*-band image of NGC 4138 after subtraction of the global exponential disk. The image is deprojected to the face-on view with the line of nodes aligned horizontally.

$R = 21''$, which coincides exactly with the H II ring noted by Pogge & Eskridge (1987); the brightness distribution is not uniform along the ring, and its shape is not perfectly circular. We also constructed a $B-R$ color map, which shows the ring to be a very blue feature; a red half-ring at $R = 15''$ borders the inner southeastern edge of the blue ring, and spiral arms emerge from its outer edge and end at another red ring at $R \approx 35''$. Outside $R = 35''$ the global disk is featureless.

The residual *K*-band map shows an almost spherical bulge inside $R = 8''$ (Fig. 8); this region is also distinguished by high stellar velocity dispersion, which exceeds 100 km s^{-1} (Jore et al. 1996). However, although the inner feature of NGC 4138 is an obvious bulge, its radial brightness profile can be well fitted to an exponential law with $r_0 = 1''.6$ and $K_0 = 14.2$ and cannot be satisfactorily fitted to de Vaucouleurs law, which should be more appropriate for the bulge of an early-type galaxy. Jore et al. (1996) obtained the same result: they report an exponential bulge with a scale length of $1''.9 \pm 0''.1$ from the analysis of an *I*-band image of NGC 4138.

4. NGC 4550

4.1. *Lick Indices in the Central Part*

Our two-dimensional distributions of Lick indices and azimuthally averaged radial variations of indices in NGC 4550 are based on three sets of wide-field spectroscopic data, including two original ones obtained with the old and new variants of the MPFS and the third set obtained with the SAURON instrument. Therefore we compare in Figure 9 the radial profiles of indices based on all three data sources. Also plotted are two integrated values—the Mg *b* and Fe 5335 indices—in the central $2'' \times 4''$ aperture and the Mg *b* index in the bulge ($4'' \pm 2''.5$ from the center along the minor axis) adopted from Fisher et al. (1996). The agreement is excellent after proper index calibration, with no significant

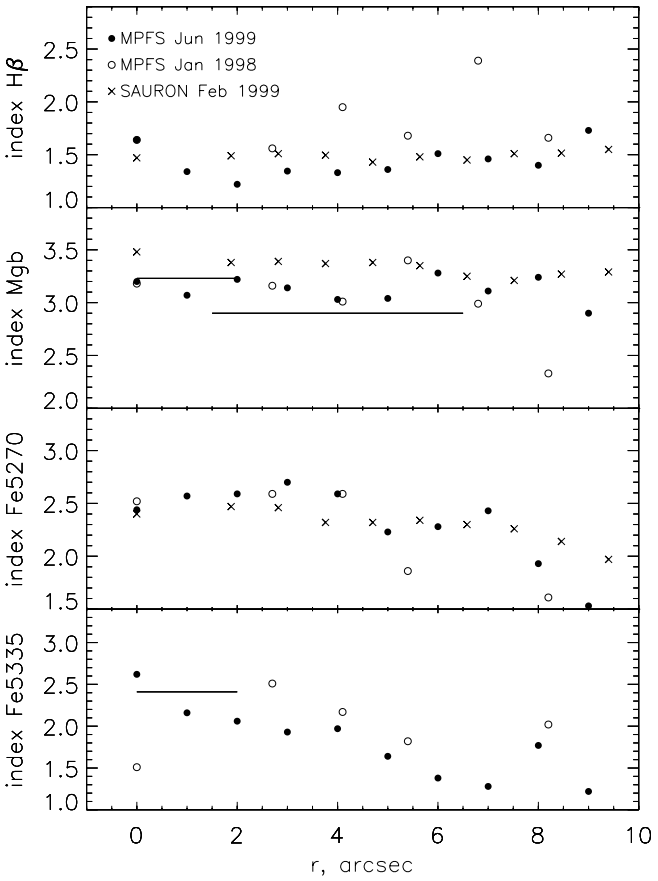

FIG. 9.—Comparison of two MPFS and one SAURON sets of index measurements for NGC 4550. Two-dimensional measurements are azimuthally averaged over concentric rings centered on the nucleus. Also plotted are the long-slit data of Fisher, Franx, & Illingworth (1996) taken along the major ($r = 0''$–$2''$) and minor ($r = 1''.5$–$6''.5$) axes.

systematic shifts. We must point out only two important details: the scatter of neighboring ring estimates is maximal for the 1998 January MPFS data and the poor spatial resolution of SAURON (seeing $3''$) results in noticeable smoothing of the Hβ and Mg b profiles. We therefore consider the 1999 June MPFS data set to have the best quality among all considered here; however, although the index distributions based on SAURON data lack subtle details, they nevertheless cover a more extended area and therefore better reveal large-scale trends of stellar population properties in the center of NGC 4550. It can be seen from Figure 9 that the 1999 June MPFS data set is the only one to show a bona fide peak of the Hβ absorption-line index in the center of the galaxy; the slightly poorer resolution of the other data sets smooths this feature out completely, thereby indicating the very compact size and relative faintness of the distinct nucleus in NGC 4550. Figure 10 shows diagnostic diagrams Fe 5270 versus Mg b and Hβ versus [MgFe] $\equiv$ (Mg $b\langle$Fe$\rangle)^{1/2}$ with the evolutionary stellar population models of Worthey (1994), which are used as a reference frame for the azimuthally averaged data of the 1999 June MPFS set. Figure 10*a* demonstrates a quasi-solar magnesium-to-iron ratio for stars $7''$ from the center. The unresolved nucleus has a marginally higher Mg/Fe ratio than the circumnuclear region because of a mild depression of Fe 5270 in the very center. However, on the one hand this magnesium overabundance is very small, less than +0.1 dex, and on the other hand Fe 5335 has on the contrary a peak in the center, so the average iron index, $\langle$Fe$\rangle \equiv$ (Fe 5270 + Fe 5335)/2, is not indicative of even a small magnesium overabundance of the nucleus. Adopting the solar Mg/Fe ratio in the center of NGC 4550, we would like to use the models of Worthey (1994) to estimate the luminosity-weighted ages of the stellar populations at different radii. However, Figure 10*b* shows that all the measurements lie well below the "oldest" model sequence, implying that our measurements of the Hβ absorption-line index are strongly contaminated by the Balmer emission line. We therefore can make only qualitative conclusions or relative estimates. The point corresponding to the nucleus

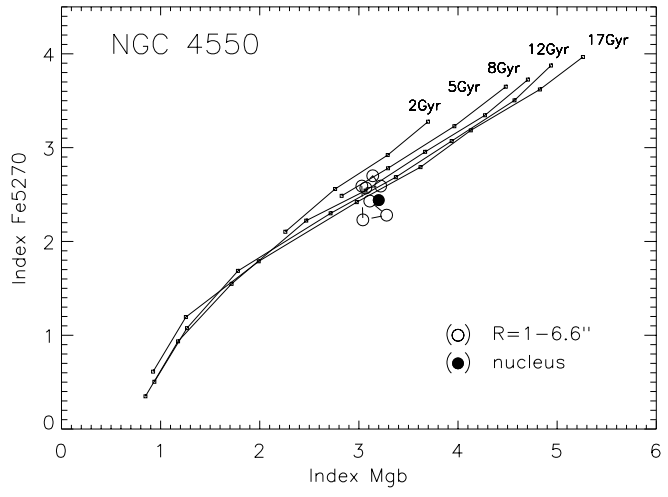

FIG. 10*a*

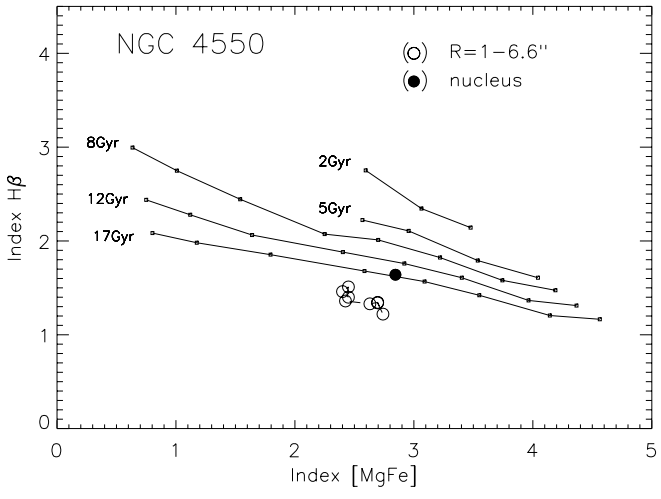

FIG. 10*b*

FIG. 10.—Diagnostic diagrams for the stellar population in the center of NGC 4550: (*a*) iron vs. magnesium diagram in which the nucleus and the azimuthally averaged MPFS 1999 June data are plotted; (*b*) hydrogen vs. metals diagram with the same data for NGC 4550. Worthey's (1994) models for old stellar populations of various ages with [Mg/Fe] = 0 are plotted as a reference; the metallicities of Worthey's models are (*right to left*) +0.50, +0.25, 0.00, −0.22, −0.50, −1.00, −1.50, and −2.00.

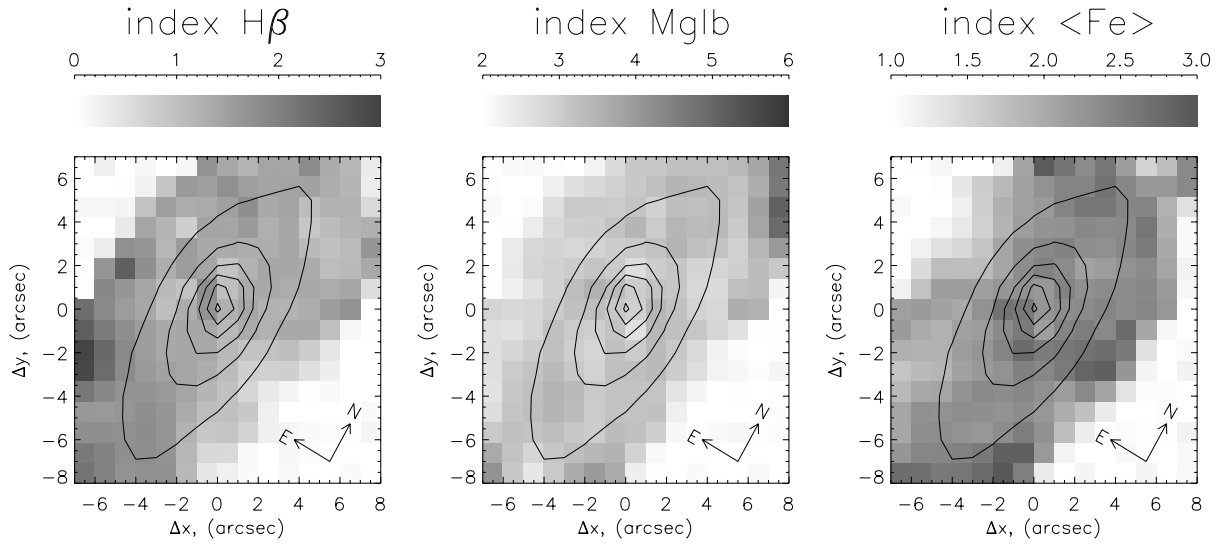

FIG. 11.—MPFS index maps for NGC 4550. Green (λ5000 Å) continuum is superposed by isophotes

stands well above the compact cloud of the circumnuclear measurements; at the same time, as we show below, emission lines, at least [O III] λ5007 and [N II] λ6583, are strongest in the nucleus, implying that the correction for the depression of Lick Hβ index due to emission must be maximal in the nucleus. This leads us to conclude that the true Hβ index in the nucleus is certainly higher than that in the surrounding region, and given that metal line indices remain approximately constant along the radius (Fig. 9), higher Hβ index should imply lower age. If interpreted in terms of the models of Worthey (1994), the 0.35 Å difference between Hβ indices in the nucleus and in the circumnuclear region implies a minimum age difference of 8 or 4 Gyr, if the average age of the nuclear stellar population is on average older or younger than 8 Gyr, respectively. The final point of this brief logical excursion is that the very compact (unresolved) nucleus of NGC 4550 is certainly distinguished by the lower mean age of its stellar population. Now the very last remark: if the nuclear stellar population is on average younger than that of the nucleus neighborhood, equal metal line indices imply higher mean metallicity in the nucleus.

The azimuthally averaged radial profiles of absorption-line indices in the center of NGC 4550 appear very smooth, flat, and almost constant, thereby casting doubt on our expectation of finding a chemically distinct nucleus in this kinematically peculiar galaxy. However, two-dimensional

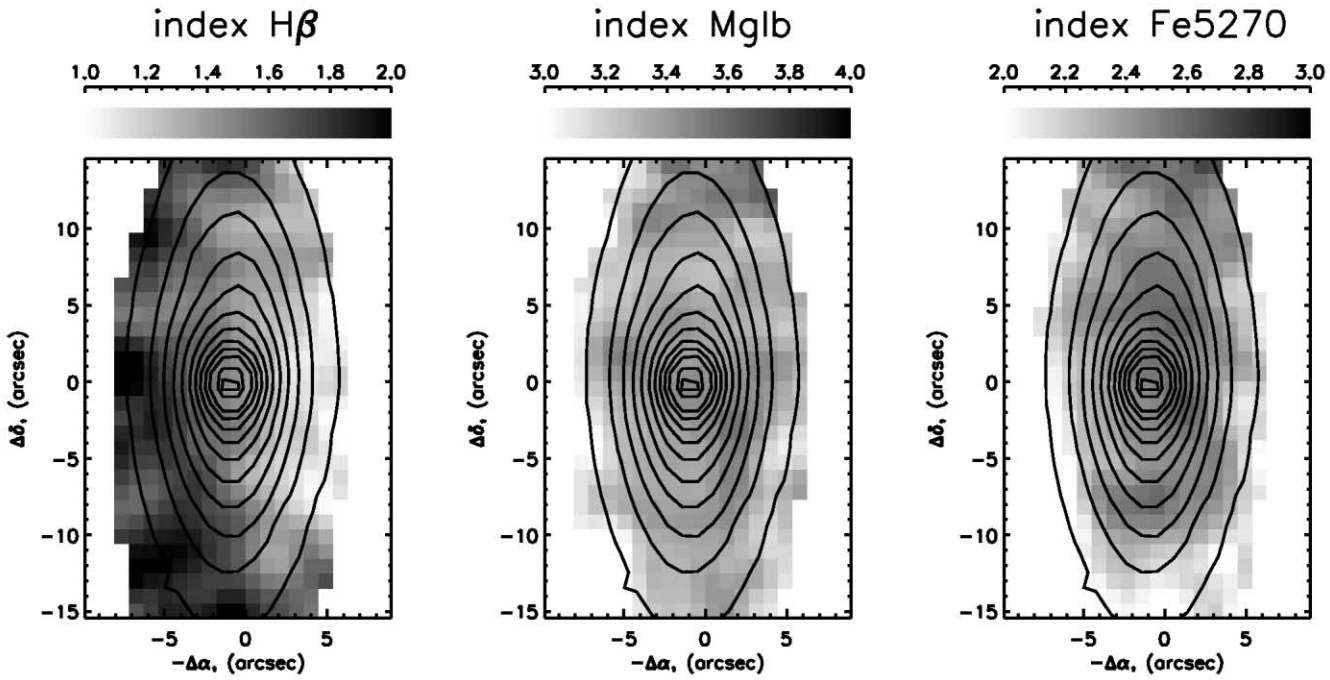

FIG. 12.—Same as Fig. 11, but SAURON index maps

distributions of the same indices reveal a very complex structure of stellar subpopulations even in the very center, within the zone of zero rotation. Figures 11 and 12 shows the index maps obtained with the new MPFS and SAURON, respectively. The former have spatial resolution twice as high as the latter because of better seeing (1.″7 versus 3.″0), and therefore the smaller element-to-element scatter of SAURON maps might be due to poorer spatial resolution; however, SAURON maps cover a larger area. One can see a $\sim 5''$-long elongated feature in the very center of Figure 11 aligned along the position angle P.A. $\sim 30^\circ$–50°. This feature is characterized by enhanced Hβ levels (indicative of the younger age of the stellar population?), as well as by higher Mg b and $\langle$Fe$\rangle$ indices (higher metallicity?). Also one can note a slight asymmetry along the east-west direction in the distributions of Hβ and $\langle$Fe$\rangle$, although it does not look very impressive. However, SAURON maps, which cover more extended areas, reveal a very conspicuous asymmetry with respect to the major axis in the distribution of the same indices: the eastern half of the galaxy shows higher Hβ and lower Fe 5270 than the western one. When the map of [O III] emission-line intensity, which is also asymmetric (Fig. 16, *left*), is taken into account, we can suggest the following interpretation for this spectacular phenomenon. We have a stellar gaseous circumnuclear disk, which is less inclined to the line of sight than the main disk of the galaxy but has approximately the same line of nodes. In this case we observe the western half of the bulge mostly through the ionized gas of this disk, resulting in a stronger contamination of the absorption-line index Hβ by emission. At the same time, the higher iron abundance of this disk, which may have formed during a prolonged secondary star formation burst, results in higher Fe 5270 index levels west of the nucleus. The spatial smoothing of SAURON data transforms the elongated Mg-rich structure in the very center of NGC 4550, which is seen in the MPFS Mg b map, into a kind of Mg-rich two-armed spiral (Fig. 12); despite the rather low contrast of this feature (ΔMg $b \approx 0.2$ Å), its regular shape looks very impressive and quite inexplicable. The direction of the Mg-enhanced minibar in the SAURON Mg b map is close to P.A. $\approx 60^\circ$ and is thus intermediate between the major and minor axes and consistent with the MPFS Mg b map.

4.2. *Central Velocity Fields of Stars and Ionized Gas*

The main peculiarity of NGC 4550 is its two equal-weighted counterrotating stellar disks, and therefore the stellar line-of-sight velocity field for this galaxy is of particular interest. Figure 13 shows the stellar velocity field for the center of NGC 4550 calculated via a formal single-Gaussian fit to the cross-correlation peaks; Figure 13 (*right*) shows the stellar velocity dispersion field obtained from the SAURON data via the same fit. As expected based on previous kinematical studies of this galaxy, the circumnuclear stellar velocity field appears very smooth and flat with no obvious signs of rotation. However, because of a higher spatial resolution of the MPFS data, a "red" spot can be seen in Figure 13 (*left*) 2.″–3.″ west of the nucleus. The asymmetry of the same sign, albeit of lower contrast, can also be seen in Figure 13 (*middle*). A formal cosine law fit to the azimuthal variations of the line-of-sight velocity gradient yields the kinematical major-axis position angles of P.A.$_0 = 310^\circ$ (MPFS) and P.A.$_0 = 300^\circ$ (SAURON) in the radius interval 1.″5–3.″0, with cosine amplitude estimates of 1.4 ± 2.3 km s^{-1} arcsec^{-1} (MPFS) and 1.0 ± 1.8 km s^{-1} arcsec^{-1} (SAURON). The corresponding position angles for the radius interval 3.″0–4.″2 are equal to P.A.$_0 = 270^\circ$ (both MPFS and SAURON), and cosine amplitudes are equal to 1.7 ± 2.2 (MPFS) and 1.4 ± 1.2 (SAURON). Although the inferred cosine amplitudes are on the order of their standard errors, the agreement of the kinematical major axis orientations based on independent observational data sets is impressive; we believe that the velocity field asymmetry is real. Recall that, according to our conclusions in § 4.1, the

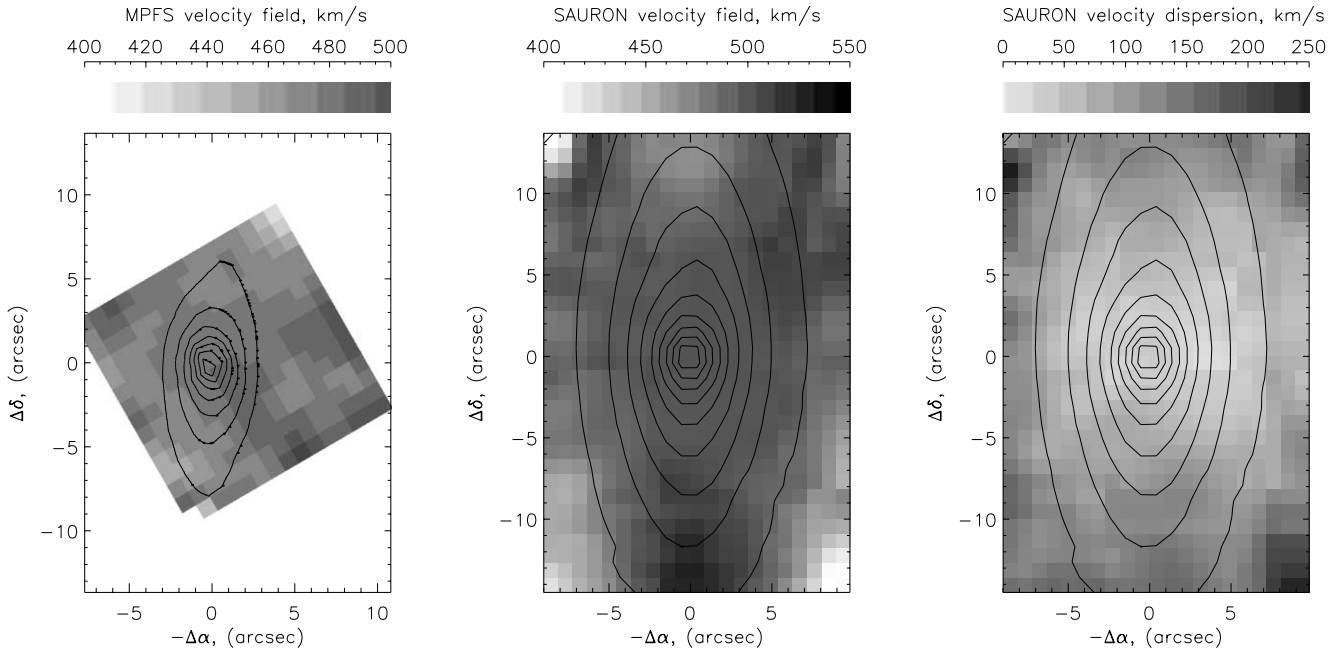

FIG. 13.—NGC 4550: Stellar line-of-sight velocities and velocity dispersion (gray scaled) calculated in the approximation of a single Gaussian LOSVD component; λ5000 Å continuum is superposed by isophotes.

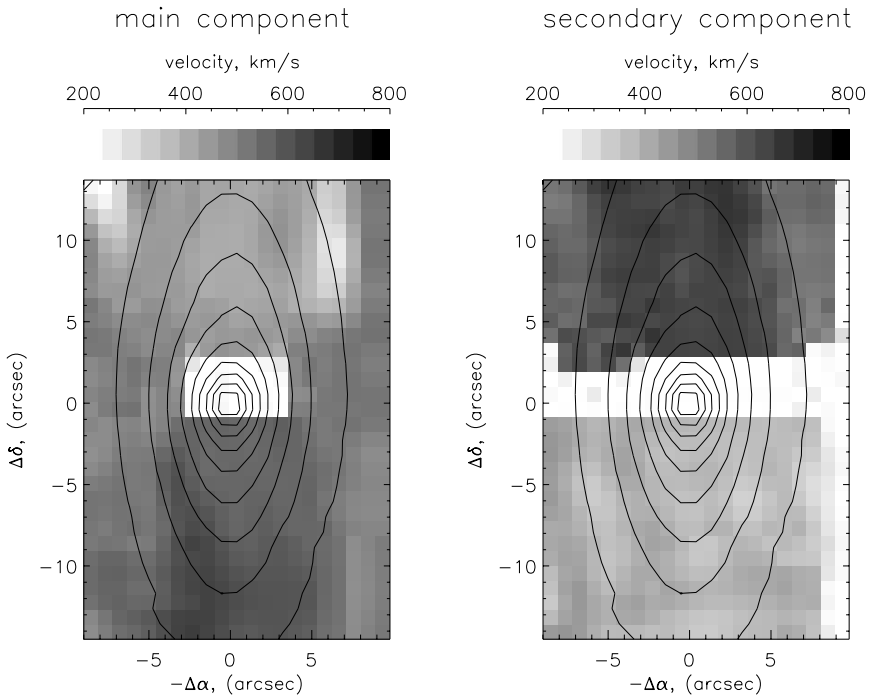

FIG. 14.—NGC 4550: Results of Gaussian decomposition of the LOSVDs based on SAURON data.

western side of the circumnuclear region is the region of the best visibility of the moderately inclined circumnuclear disk; the shallow minimum of stellar velocity dispersion seen in Figure 13 (*right*) in the same direction from the nucleus confirms this hypothesis. In a flat kinematical subsystem the cosine azimuthal dependence of line-of-sight velocities with a maximum at the P.A. orthogonal to the line of nodes implies purely radial motions. Since in this particular case the western side of the disk is the nearest to us, the "red" spot there means contraction in the inner part of the circumnuclear stellar disk with a radial velocity of about 1–3 km s^{-1}.

However, we know from the previous kinematical studies of NGC 4550 made with a long slit aligned along the major axis and with a higher spectral resolution compared with our measurements that the cross-correlation peaks in this galaxy indeed consist of two Gaussians with roughly symmetrical positions with respect to the systemic velocity of the galaxy (Rubin et al. 1992; Rix et al. 1992). We therefore performed Gaussian analysis of the cross-correlation peaks, assuming that there are two components everywhere except at the very center where the low formal stellar velocity dispersion, which implies too small a separation between the velocity components, prevents the application of this procedure. Hereafter we refer to the velocity component that is the strongest on the major axis 10″–15″ from the center (one can see corresponding light and dark spots in Fig. 13, *middle*) as "the main," and the velocity component with the opposite sense of rotation as the "secondary." Figure 14 shows the smoothed velocity fields of the main and secondary components. At first glance, they seem to be almost perfect mirror images of each other. However, a closer inspection reveals that the secondary stellar component is more extended in the east-west direction (orthogonally to the major axis) than the main one. This impression is further confirmed by the fact that in Figure 13 (*middle*), where the cross-correlation peaks are fitted by a single Gaussian, which therefore reflects the dominant kinematical component, one can see that the sense of rotation changes abruptly when it recedes east or west from the major axis by more than 6″. The appreciable extension of the secondary velocity component in the direction orthogonal to the major axis (along the z-direction) implies first and foremost its possible relation to the moderately inclined circumnuclear disk, which we feel shows up in the distributions of Lick indices.

Contrary to that in stars, the ionized gas in the center of NGC 4550 is known to rotate rather rapidly (Rix et al. 1992). We measured its two-dimensional velocity field by using two emission lines: [N II] λ6583 (the new MPFS) and [O III] λ5007 (SAURON). The results are presented in Figures 15 and 16. As expected from earlier results (Rix et al. 1992), the rotation sense of the ionized gas generally agrees with that of the secondary stellar component: the northern half of the disk is receding. This agreement confirms our idea that the secondary stellar velocity component is related to the circumnuclear stellar gaseous disk. But the new detail is that the kinematical major axis of the ionized gas is not aligned with the major axis of continuum isophotes. A cosine law fit to the azimuthal variations of the line-of-sight velocity gradients within $R = 3''$ yields $\mathrm{P.A.}_0 = 40^\circ$ and the projected angular rotation velocity $\omega \sin i = 32.3 \pm 13.0$ km s^{-1} arcsec^{-1} (MPFS data), and $\mathrm{P.A.}_0 = 17^\circ$ and $\omega \sin i = 15.5 \pm 3.8$ km s^{-1} arcsec^{-1} (SAURON data); the MPFS data, which have higher spatial resolution, imply a local extremum of rotation velocity in 3″– 4″ galactocentric distance interval. The direction of the turn of the kinematical major axis of the gas component coincides with the orientation of the Mg-enhanced feature in the center of NGC 4550. However, the fact that the major axis of contin-

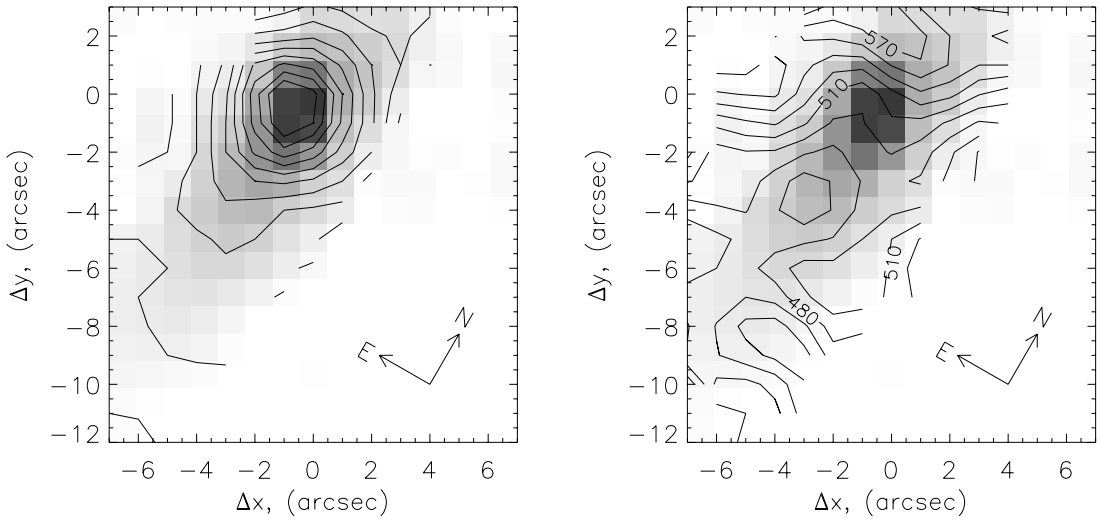

FIG. 15.—NGC 4550: [N II] λ6583 emission brightness distribution (*left*, *isolines*) and the line-of-sight velocity field of ionized gas (*right*, *isolines*) superposed on the red (λ6500 Å) continuum (gray scaled) from the MPFS data.

uum isophotes exhibits no similar turn in the center of the galaxy might mean that the kinematics of the gas is indicative of a triaxial (bar) structure, which does not show up in the morphology because of the edge-on orientation of the entire galaxy. A global bar in NGC 4550 should inevitably manifest itself in the form of the radial stellar motions mentioned above.

5. DISCUSSION

Both NGC 4138 and NGC 4550 are lenticular galaxies with lower than intermediate luminosity (Table 1) and small bulges, which is quite untypical for early-type disk galaxies. The bulge of NGC 4138 is undoubtedly exponential, whereas the situation with the bulge of NGC 4550 is less clear and requires further discussion.

5.1. *Minor Mergers?*

In § 1 we reviewed the history of bulge-disk decomposition in NGC 4550 and mentioned that the results were ambiguous. The complexity of this procedure when applied to NGC 4550 is due to the edge-on orientation and early

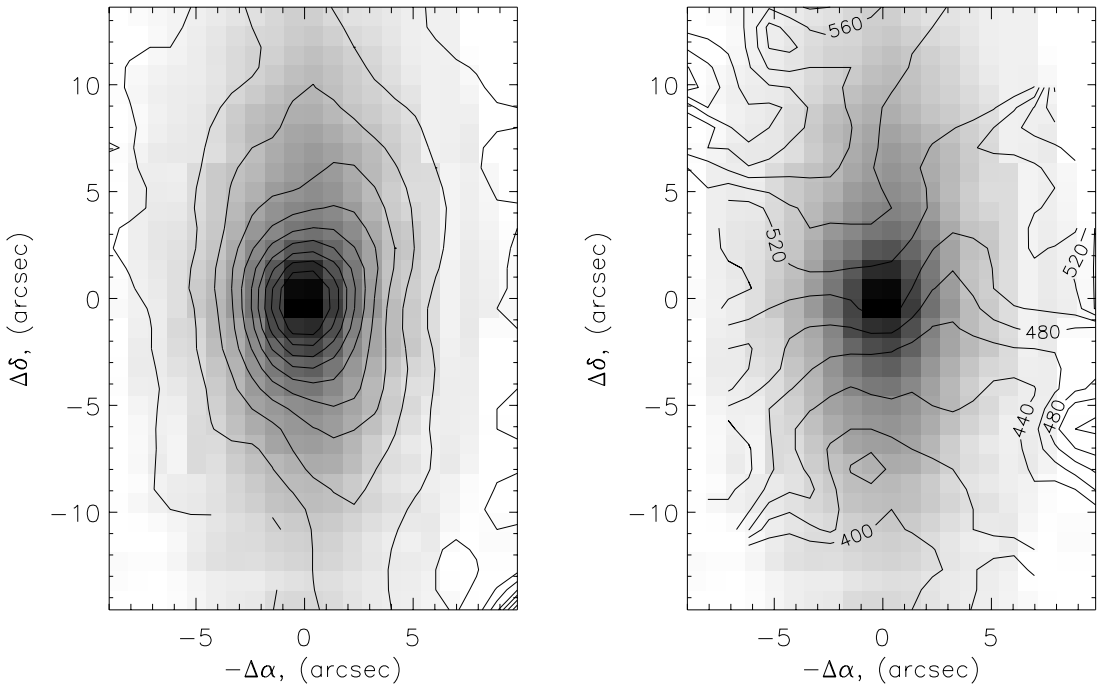

FIG. 16.—NGC 4550: [O III] λ5007 emission brightness distribution (*left*, *isolines*) and the line-of-sight velocity field of ionized gas (*right*, *isolines*) superposed on the green (λ5000 Å) continuum (gray scaled) from the SAURON data.

morphological type of the galaxy, which implies that the stellar disk is thick and therefore prevents the application of the usual approach when the bulge brightness profile is successfully inferred from the minor axis cross section. Another method for decomposing edge-on lenticular galaxies into bulge and disk components was first proposed by Simien & Michard (1990) and later by Scorza et al. (1998). It involves the construction of the radial profile of the fourth Fourier cosine coefficient, a_4, of azimuthal brightness variations and is based on the assumption that bulges have purely elliptical isophotes. The idea is to subtract an edge-on disk component with a positive a_4, which is assumed to be superposed on a spheroidal bulge, until residual brightness isophotes become pure ellipses. Needless to say, this method does not work with galaxies that have peanut-shaped (boxy) bulges. But even if it works and yields something with purely elliptical isophotes as the final product of decomposition, we cannot be sure that the residual distribution is that of a bulge. Let us imagine for an instant that we have two flat circular disks with different inclinations; then, after subtracting the disk with the more edge-on orientation by using the above method, we obtain the brightness distribution of the second, more face-on disk, as the residual, and its isophotes would be pure ellipses. We believe this to be the case in NGC 4550. The component of NGC 4550 that is photometrically dominant in the central part cannot be a bulge: we see no clear bulge signatures in its kinematics. The low stellar velocity dispersion of both counterrotating components proves them to be disks. The fact that the relative intensity of two counterrotating stellar components varies along the z-axis (in the direction orthogonal to the line of nodes) is indicative of different inclinations.

Adopting the hypothesis of two stellar disks with different inclinations for NGC 4550 allows us to reinterpret the brightness profiles of the decomposed components obtained by Scorza et al. (1998): the component that they considered to be a bulge with a quasi–de Vaucouleurs profile resembles in fact two exponential segments with different scale lengths and may be a moderately inclined two-tier disk. Disks with two exponential scale lengths exist—we have recently found several such disks in galaxies with chemically distinct nuclei—NGC 5533 (Sil'chenko, Burenkov, & Vlasyuk 1997a), NGC 7217 (Sil'chenko & Afanasiev 2000), and NGC 615 (Sil'chenko, Vlasyuk, & Alvarado 2001). We proposed a new scenario to associate the origin of these global multitier disks with that of chemically distinct nuclei and thereby with secondary bursts of nuclear star formation. Our scenario involves catastrophic radial redistribution of gas in global disks of galaxies during minor merger events, which in addition triggers secondary bursts of star formation. According to Lin & Pringle (1987), the exponential scale length of a gradually forming stellar disk is determined by the initial size of its gaseous progenitor, implying that the catastrophic compression of the global gas distribution toward the center of a galaxy at any intermediate epoch accompanied by continued global star formation would produce a global stellar disk with two exponential scale lengths. Minor mergers are the most popular explanation of the origin of counterrotating stellar components (Thakar & Ryden 1996, 1998), and therefore such an event may indeed have produced a two-tier global disk in NGC 4550, provided that the global disk of the galaxy still retained some primordial gas at the time of the minor merger. The secondary gas of the infalling satellite with a different angular momentum may in turn provide the material for the formation of another disk with a different inclination.

5.2. *Triaxial Potential?*

A global bar may provide an alternative mechanism for throwing gas toward the center and possibly inducing some counterrotation in the stellar component (Athanassoula 1996; Wozniak & Pfenniger 1997). Although NGC 4138 is classified as an unbarred galaxy and one can hardly expect to note a bar in NGC 4550 because of its edge-on orientation, both galaxies nevertheless exhibit some characteristic features that are usually associated with bars. A prominent H II ring at $R = 21''$ in NGC 4138, which we also found to be accompanied by red and IR continuum enhancement, is a typical signature of the inner Lindblad resonance in a triaxial potential (Buta & Crocker 1993). The significant large-scale warp of the kinematical major axis of neutral gas observed in this galaxy (Kornreich et al. 2001) leads us to conclude that the dark halo around NGC 4138 is also triaxial.

As for NGC 4550, the diversity of rotation curves of two counterrotating stellar disks inside $R = 8''$ is difficult to explain without invoking bar effects. In the axisymmetric case both stellar disks, which are dynamically cold, if observed along the line of nodes should exhibit purely circular velocities determined by the (common) gravitational potential. The major-axis cross sections of the line-of-sight velocity fields of both stellar components should therefore appear similar if transformed into absolute rotation velocities that differ only by a factor of $\sin i_1/\sin i_2$. Figure 17 shows rotation curves of both counterrotating stellar disks of NGC 4550, based on the SAURON data: we used relative velocities (with respect to the nucleus) along P.A. $= 178°$ and mirrored the negative values into the positive ones. The rotation curves can be seen to be quite different at $R < 8''$, with the rotation velocity of the main component increasing slowly and quasi-linearly up to a radial distance of $R = 10''$, whereas the secondary compo-

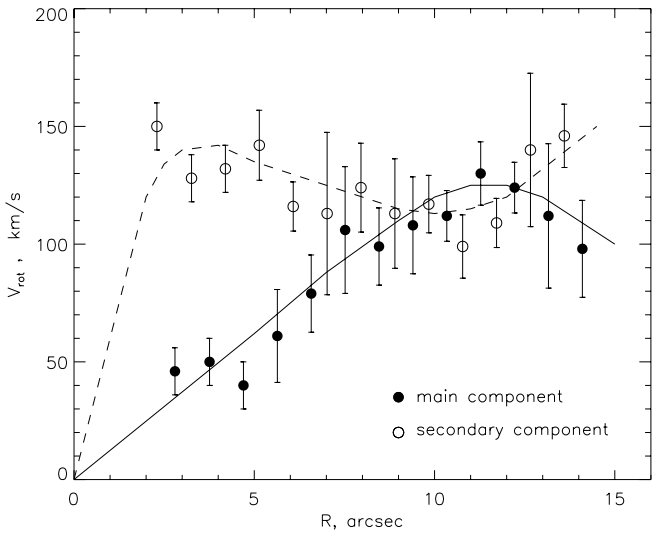

FIG. 17.—Rotation curves (multiplied by unknown factors of $\sin i_{m,s}$) of the main and secondary stellar velocity components in NGC 4550 inferred from the major-axis cross sections of the maps in Fig. 14.

nent reaches its maximum rotation velocity at the inner edge of the area decomposed. Rix et al. (1992) obtained the same pattern of rotation velocities, without, however, discussing it. Both disks are in the common gravitational field with the same potential, and therefore discrepant rotation velocities at the major axis are indicative of noncircular motions in at least one of the disks. Flat rotation curves are commonly obtained if measured along major axes of bars, and we therefore suggest that the bar is hosted by the main disk.

There is yet another property of bars, which was predicted theoretically and can be now confirmed observationally: Friedli & Benz (1993) showed via dynamical numerical simulations that counterrotating gas fueled toward the center in a barred potential populates an *inclined* plane where it remains for a long time as a thin stable fast-rotating circumnuclear disk. Both galaxies considered here exhibit such a warp of the gaseous rotation planes near the center: in NGC 4550 the circumnuclear gaseous disk is inclined with respect to the main symmetry plane of the galaxy by about 20°–40°, whereas in NGC 4138 we observe a turn of the kinematical major axis of the ionized gas component within $R \approx 5''$ from the center, which is consistent with the apparent orientation of the central gas-dust distribution. However, the exact orientation of the circumnuclear gas rotation plane remains ambiguous because of the projection effect. Since the gas located at greater galactocentric distances in NGC 4138 is probably confined to the plane of the main disk (Jore et al. 1996; Haynes et al. 2000), triaxial potential seems to be the most natural explanation for the inclined circumnuclear disk of counterrotating gas, at least in this galaxy. As for the mutual inclination of the counterrotating disks in NGC 4550, it may be due to the initial orientation of the angular momentum of the accreting gas, as well as to the subsequent effect of the bar potential. However, the observed marginal discrepancy of the rotation axes of ionized gas and secondary stellar component in the very center of the galaxy might imply that both factors are involved.

5.3. *Concluding Remarks*

After all, what is the answer to the question at the beginning of this paper? Are chemically distinct nuclei mandatory features in galaxies with multiple kinematical subsystems? Or, in other words, does there exist a single event that simultaneously produces extended kinematically decoupled subsystems and centrally concentrated secondary bursts of star formation?

To sum up our discussion of the galaxies considered, we conclude that in NGC 4138 the nucleus is certainly chemically distinct, with the central concentration of magnesium enhancement marginally exceeding that of iron. The same pattern is observed in two other galaxies with stellar counterrotation: NGC 7217 (Sil'chenko & Afanasiev 2000) and NGC 7331 (Sil'chenko 1999b). NGC 4550 exhibits complex extended structures in its center that manifest themselves in mildly enhanced levels of magnesium and iron indices; the stellar population in the unresolved nucleus is younger (on the average) than that in its outskirts. This leads us to conclude that although NGC 4550 does not possess a chemically distinct nucleus in the sense defined previously, there are clear signatures of a secondary burst of star formation, which was possibly confined to the counterrotating stellar gaseous disk seen more face-on than the main disk of the galaxy.

As for a single event that may have produced all the peculiar phenomena discussed above, must it certainly be a minor merger? Recently an interesting hypothesis was proposed: Aguerri, Balcells, & Peletier (2001) suggest that initially all bulges in spiral galaxies have exponential (surface) density profiles and only after accreting a dense satellite some of them acquire the classic de Vaucouleurs shape. Although the particular numerical simulations performed by the above authors confirm such an evolutionary scenario, it seems to us that much depends on the amount of dissipation. Our observational finding of the relation between chemically distinct nuclei and exponential brightness profiles in the bulges of the *early-type* disk galaxies NGC 7217 and NGC 4138 (plus several cases of isolated compact inner disks) is rather indicative of highly dissipative evolution of disk galaxies involving catastrophic radial redistribution of gas after a possible minor merger event. Such a path of secular evolution is likely to result in exponential profile inner structures. However, whether a minor merger is indeed needed to cause the catastrophic radial redistribution of gas and produce counterrotating subsystems is still an open question. All these consequences may be a result of a transient large-scale bar.

Transient bars are very promising objects for the hypothesis of galaxy secular evolution and for our particular cases of galaxies with counterrotating stellar disks. First of all, bars provoke gas inflow into the center, providing a supply for the central star formation bursts. Secondly, a counterrotating stellar component can also be formed by a slow evolution of a triaxial potential: for example, Evans & Collett (1994) explain counterrotation in NGC 4550 by the dissolution of a bar, and Tremaine & Yu (2000) have proposed a triaxial halo slowly changing its rotation as a possible cause of retrograde disk orbits in flattened galaxies that is applicable to NGC 4138. Perhaps in NGC 4550 the global bar still exists, because its kinematics is very typical for a triaxial potential, and the absence of a prominent chemically distinct nucleus may be evidence of persistent bar influence: it is known that bars smooth all the metallicity variations over the radius (Martin & Roy 1994).

Certainly, a transient bar may be a by-product of minor mergers or even of a mere galaxy interaction, and therefore the two mechanisms may be closely related. However, we cannot rule out possible spontaneous large-scale bar instabilities in young disks of forming spiral galaxies.

We thank V.V. Vlasyuk and the postgraduate student of the Special Astrophysical Observatory, A. V. Moiseev, for supporting the observations at the 6 m telescope. The 6 m telescope is operated with financial support from the Science Ministry of Russia (registration 01-43). We also thank the Programme Committee of the 6 m telescope for allocating observational time. During our data analysis we used the Lyon-Meudon Extragalactic Database (LEDA) supplied by the LEDA team at the CRAL-Observatoire de Lyon (France) and the NASA/IPAC Extragalactic Database (NED) operated by the Jet Propulsion Laboratory, California Institute of Technology under contract with the National Aeronautics and Space Administration. The work is partially based on the data taken from the ING Archive of the UK Astronomy Data Centre and on observations

made with the NASA/ESA *Hubble Space Telescope*, obtained from the data archive at the Space Telescope Science Institute. STScI is operated by the Association of Universities for Research in Astronomy, Inc., under NASA contract NAS 5-26555. The study of chemically distinct nuclei in galaxies with multiple kinematical subsystems was supported by the Russian Foundation for Basic Research (grant 98-02-16196) and the Russian State Scientific Technical Program, Astronomy: Basic Space Research (astronomy section), grant 1.2.4.1.

REFERENCES

Afanasiev, V. L., Dodonov, S. N., Drabek, S. V., & Vlasyuk, V. V. 1996, MPFS Manual (Nizhnij Arkhyz: SAO Publ.)
Afanasiev, V. L., & Sil'chenko, O. K. 1999, AJ, 117, 1725
Aguerri, J. A. L., Balcells, M., & Peletier, R. F. 2001, A&A, 367, 428
Athanassoula, E. 1996, in ASP Conf. Ser. 91, Barred Galaxies, ed. R. Buta, D. A. Crocker, & B. G. Elmegreen (San Francisco: ASP), 309
Bacon, R., et al. 1995, A&AS, 113, 347
———. 2001, MNRAS, 326, 23
Baggett, W. E., Baggett, S. M., & Anderson, K. S. J. 1998, AJ, 116, 1626
Buta, R., & Crocker, D. A. 1993, AJ, 105, 1344
Caon, N., Capaccioli, M., & D'Onofrio, M. 1993, MNRAS, 265, 1013
Cardiel, N., Gorgas, J., Cenarro, J., & Gonzalez, J. J. 1998, A&AS, 127, 597
de Zeeuw, P. T., et al. 2002, MNRAS, 329, 513
Evans, N. W., & Collett, J. L. 1994, ApJ, 420, L67
Fisher, D., Franx, M., & Illingworth, G. 1996, ApJ, 459, 110
Fisher, D., Illingworth, G., & Franx, M. 1994, AJ, 107, 160
Freeman, K. C. 1970, ApJ, 160, 811
Friedli, D., & Benz, W. 1993, A&A, 268, 65
Gavazzi, G., Franzetti, P., Scodeggio, M., Boselli, A., Pierini, D., Baffa, C., Lisi, F., & Hunt, L. K. 2000, A&AS, 142, 65
Haynes, M., Jore, K. P., Barrett, E. A., Broeils, A. H., & Murray, B. M. 2000, AJ, 120, 703
Jore, K. P., Broeils, A. H., & Haynes, M. P. 1996, AJ, 112, 438
Kornreich, D. A., Haynes, M. P., Jore, K. P., & Lovelace, R. V. E. 2001, AJ, 121, 1358
Lin, D. N. C., & Pringle, J. E. 1987, ApJ, 320, L87
Martin, P., & Roy, J.-R. 1994, ApJ, 424, 599
Merrifield, M. R., & Kuijken, K. 1994, ApJ, 432, 575
Plana, H., & Boulesteix, J. 1996, A&A, 307, 391
Pogge, R. W., & Eskridge, P. B. 1987, AJ, 93, 291
Prada, F., Gutierrez, C. M., Peletier, R. F., & McKeith, C. D. 1996, ApJ, 463, L9
Rix, H.-W., Franx, M., Fisher, D., & Illingworth, G. 1992, ApJ, 400, L5
Rix, H.-W., Kennicutt, R. C., Jr., Braun, R., & Walterbos, R. A. M. 1995, ApJ, 438, 155
Rubin, V. C. 1994, AJ, 107, 173
Rubin, V. C., Graham, J. A., & Kenney, J. D. P. 1992, ApJ, 394, L9
Scorza, C., Bender, R., Winkelmann, C., Capaccioli, M., & Macchetto, D. F. 1998, A&AS, 131, 265
Sil'chenko, O. K. 1994, AZh, 71, 706
———. 1996, AZh Pis'ma, 22, 124
———. 1999a, AJ, 117, 2725
———. 1999b, AJ, 118, 186
———. 2000, AJ, 120, 741
Sil'chenko, O. K., & Afanasiev, V. L. 2000, A&A, 364, 479
Sil'chenko, O. K., Afanasiev, V. L., & Vlasyuk, V. V. 1992, AZh, 69, 1121
Sil'chenko, O. K., Burenkov, A. N., & Vlasyuk, V. V. 1997a, NewA, 3, 15
Sil'chenko, O. K., Vlasyuk, V. V., & Alvarado, F. 2001, AJ, 121, 2499
Sil'chenko, O. K., Vlasyuk, V. V., & Burenkov, A. N. 1997b, A&A, 326, 941
Simien, F., & Michard, R. 1990, A&A, 227, 11
Thakar, A. R., & Ryden, B. S. 1996, ApJ, 461, 55
———. 1998, ApJ, 506, 93
Tremaine, S., & Yu, Q. 2000, MNRAS, 319, 1
Vlasyuk, V. V. 1993, Bull. Spec. Astrophys. Obs., 36, 107
Worthey, G. 1994, ApJS, 95, 107
Worthey, G., Faber, S. M., & Gonzalez, J. J. 1992, ApJ, 398, 69
Worthey, G., Faber, S. M., Gonzalez, J. J., & Burstein, D. 1994, ApJS, 94, 687
Wozniak, H., & Pfenniger, D. 1997, A&A, 317, 14
Zasov, A. V., & Sil'chenko, O. K. 1997, AZh, 74, 824